Infrared Spectra of the CH_3-MX and CH_2-MHX Complexes Formed by Reactions of Laser-Ablated Group 3 Metal Atoms with Methyl Halides

Han-Gook Cho and Lester Andrews*

Department of Chemistry, University of Incheon, 177 Dohwa-dong, Nam-ku, Incheon, 402-749, South Korea, and Department of Chemistry, University of Virginia, P. O. Box 400319, Charlottesville, Virginia 22904-4319

Received: November 17, 2006; In Final Form: December 27, 2006

Reactions of laser-ablated group 3 metal atoms with methyl halides have been carried out in excess of Ar during condensation and the matrix infrared spectra studied. The metals are as effective as other early transition metals in providing insertion products (CH_3-MX) and higher oxidation state methylidene complexes (CH_2-MHX) (X = F, Cl, Br) following α-hydrogen migration. Unlike the cases of the group 4−6 metals, the calculated methylidene complex structures show little evidence for agostic distortion, consistent with the previously studied group 3 metal methylidene hydrides, and the C−M bond lengths of the insertion and methylidene complexes are comparable to each other. However, the C−Sc bond lengths are 0.013, 0.025, and 0.029 Å shorter for the CH_2-ScHX complexes, respectively, and the spin densities are consistent with weak C(2p)−Sc(3d) π bonding. The present results reconfirm that the number of valence electrons on the metal is important for agostic interaction in simple methylidene complexes.

Introduction

Unlike the cases of other transition metals, group 3 metal complexes with C−M bond are rare, partly due to the small number of valence electrons, which limits the number of ligands and electron back-donation to the ligand π^*-orbitals.[1] Bulky substituents are normally needed to stabilize the structure.[2] Reactions of group 3 metals with small organic molecules have not been studied often, and only a few complexes have been identified from reactions of the cations with small alkanes.[3] Preparation of group 3 metal complexes with C−M bonds (e.g., RCH_2-MX or RCH−MXY) is still a challenge.

There have been theoretical studies for the reactions of group 3 metals with small organic molecules and the plausible products. Seigbahn et al. predicted in their investigation on the reactions of the second row transition metals with alkanes that yttrium would not be very reactive.[4] They also explored the possibilities of metal halide reactions with small alkanes.[5] Dobado et al. suggested a distorted CH_2 group in $ScCH_2$ in a study of MCH_n (M = K−Mn, $n = 1-3$).[6] The binding energies and structures of $M-CH_2$, M−CHF, and $M-CF_2$ of the first row transition metals were reported by Dalmázio and Duarte.[7] Bonding of the first- and second-row transition-metal cations to methylidene ($:CH_2$) was analyzed by Bauschlicher et al.[8]

Reactions of laser-ablated early transition-metal atoms with methane and methyl halides have recently introduced a new class of small complexes with a carbon−metal bond.[9−15] Particularly the high oxidation state products with multiple carbon−metal bonds are relevant model systems for much larger high oxidation state transition-metal complexes, which often have important catalytic properties for methathesis reactions of alkenes, alkynes, and cyclic compounds.[16] The small methylidene complexes normally possess agostically distorted structures and many of the systems also show fascinating photochemistry, including persistent photoreversibility and dramatic product increases.[15]

Recently the first preparation of group 3 metal methylidene dihydrides has been developed from reactions with CH_4.[17] Group 3 metals are just as effective as other early transition metals in C−H bond activation and the following α-hydrogen migration. Interestingly enough, the structures are highly symmetrical (no agostic distortion), unlike other early transition-metal methylidene dihydrides.[15] The C−M bond length of CH_2-MH_2 is comparable to that of CH_3-MH, indicating that the methylidene C−M bond is essentially a single bond. The symmetrical structures and relatively long C−M bonds in the methylidene complex are traced to the small number of valence electrons of the group 3 metals.

Previous studies show that methyl halides normally give higher product yields in reaction with early transition metals and show progressive variations in vibrational characteristics and molecular structures with the halide substituent,[9−11] corroborating the reactions with methane. We, therefore, have carried out reactions of group 3 metals with CH_3X molecules (X = F, Cl, and Br) diluted in argon, and the products are identified from the matrix infrared spectra. The insertion and methylidene products are formed during deposition and photolysis afterward, while the yields vary dramatically from system to system. Consistent structural characteristics of the products are observed, and in several systems, photoreversibility is found. Products are identified by the effect of isotopic substitution on the infrared spectrum and complementary density functional theory (DFT) frequency calculations.

Experimental and Computational Methods

Laser-ablated group 3 metal atoms (Johnson-Matthey) were reacted with CH_3X isotopomers ((CH_3F, CH_3Cl, and CH_3Br (Matheson), CD_3F (synthesized from CD_3Br and HgF_2), $^{13}CH_3F$, CD_3Br (Cambridge Isotopic Laboratories, 99%), and CD_3Cl (synthesized from CD_3Br and $HgCl_2$)) in excess argon during

* To whom correspondence should be addressed. E-mail: lsa@virginia.edu.

10.1021/jp067662g CCC: $37.00
Published on Web 03/09/2007

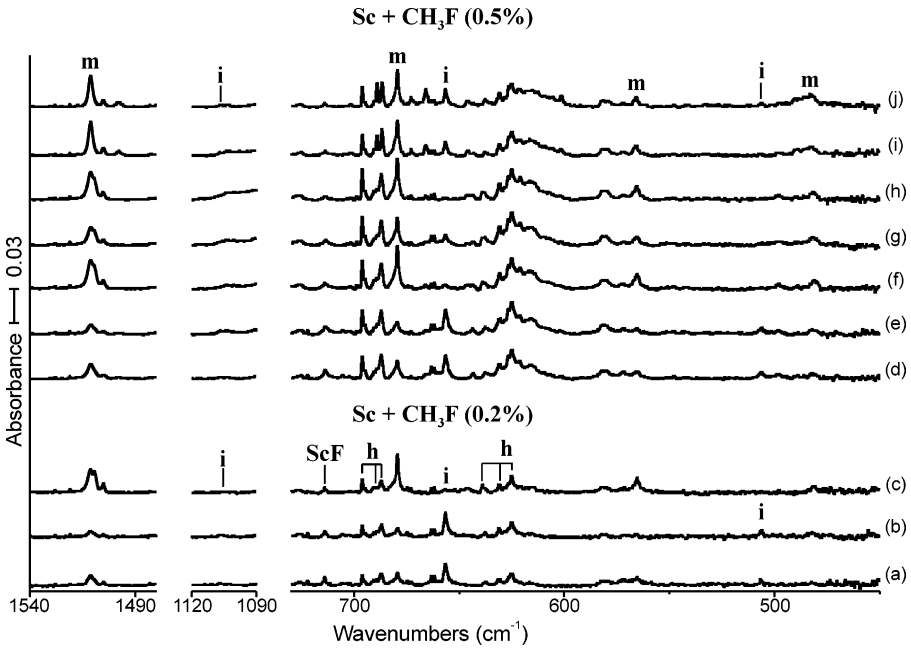

Figure 1. IR spectra in the regions of 1480−1540, 1090−1120, and 450−730 cm^{-1} for laser-ablated Sc atoms co-deposited with CH_3F in excess argon at 8 K. (a) Sc + 0.2% CH_3F in Ar co-deposited for 1 h. (b) After broad-band photolysis with a filter (λ > 420 nm). (c) After broad-band photolysis with a filter (240 < λ < 380 nm). (d) Sc + 0.5% CH_3F in Ar co-deposited for 1 h. (e) After broad-band photolysis with a filter (λ > 420 nm). (f) After broad-band photolysis with a filter (240 < λ < 380 nm). (g) After broad-band photolysis with a filter (λ > 420 nm). (h) After broad-band photolysis with a filter (240 < λ < 380 nm). (i) After annealing to 28 K. (j) After annealing to 36 K. **i**, **m**, and **h** denote the product absorption groups.

condensation at 8 K using a closed-cycle refrigerator (Air Products HC-2). The methods have been described in detail elsewhere.[18,19] Concentrations of gas mixtures are typically 0.2−0.5% in argon. After reaction, infrared spectra were recorded at a resolution of 0.5 cm^{-1} using a Nicolet 550 spectrometer with an MCT-B detector. Samples were later irradiated by a mercury arc lamp (175 W) with a combination of optical filters for 20 min periods and were annealed, and more spectra were recorded.

Complementary DFT calculations were carried out using the Gaussian 03 package,[20] B3LYP density functional,[21] 6-11++G-(3df,3pd) basis sets for C, H, F, Cl, Br, and Sc[22] and SDD pseudopotential and basis set[23] for Y and La to provide a consistent set of vibrational frequencies for the reaction products. Geometries were fully relaxed during optimization, and the optimized geometry was confirmed by vibrational analysis. Fine grid gives virtually the same results as ultrafine grid computations. Anharmonic frequency calculations using numerical differentiation[24] (with Gaussian 03 keyword "anharmonic") were also carried out with B3LYP to compare with experimental values and to examine the effects of anharmonicity. Additional BPW91,[25] MP2,[26] and CCSD[27] calculations were done to substantiate the B3LYP results. All of the vibrational frequencies were calculated analytically. In the calculation of binding energy of a metal complex, the zero-point energy is included.

Results and Assignments

Reactions of Sc, Y, and La with methyl halide isotopomers were carried out in condensing argon, and the observed product vibrational characteristics and their variations upon photolysis and annealing are compared with the calculated results.

Sc + CH_3X. The IR spectra from reactions of laser-ablated Sc atoms with CH_3F and CD_3F are shown in Figures 1 and 2. Three sets of product absorptions marked "**i**" (for insertion product), "**m**" (for methylidene), and "**h**" (for higher-order product) are observed on the basis of the behaviors upon photolysis and annealing, and the observed frequencies are listed in Table 1. The Sc + CH_3F spectra in the regions of 1480−1540, 1090−1120, and 450−710 cm^{-1} are shown in Figure 1, which includes the original spectra after co-deposition with 0.2 (a) and 0.5% (d) CH_3F and their variations upon photolysis and annealing (b,c,e−j).

The absorptions marked **i** increase about 20% upon visible (λ > 420 nm) irradiation (b and e), while the absorptions marked **m** decrease about 50% as shown in Figure 1. The **m** absorptions, however, quadruple on UV (240 < λ < 380 nm) irradiation (c and f), while the **i** absorptions virtually disappear. In the following visible irradiation (g), the **i** absorptions reappear with about 30% of the original intensity and the **m** absorptions become halved again. In the next UV irradiation (h), the **m** absorptions double in intensity and the **i** absorptions disappear again. On annealing, the **m** absorptions sharpen and later decrease (i and j), and the **i** absorptions, on the other hand, reappear.

Clearly the **i** and **m** absorptions are photoreversible; an increase of the **i** absorptions is accompanied with a decrease of the **m** absorptions on visible irradiation and vice versa on UV irradiation. However, on repeating the photoreversible cycles, the intensities of **i** absorptions tend to decrease, indicating that the conversion on UV photolysis is more effective than the reverse rearrangement on visible photolysis. Similar spectral variations upon photolysis and annealing are also observed in the Sc + CD_3F spectra shown in Figure 2. The absorptions marked with **h** increase slightly (~10% in total) in the process of photolysis and annealing but do not show any dramatic variation in intensity. However, the **h** absorptions increase substantially at high concentration of CH_3F, indicating a higher-order product.

The strong **m** absorption at 1511.2 cm^{-1} appears in a relatively clean region of the spectrum and shows essentially no ^{13}C shift but a D shift of −421.5 cm^{-1} (H/D ratio of 1.387), indicating that this is a Sc−H stretching absorption. The Sc−H

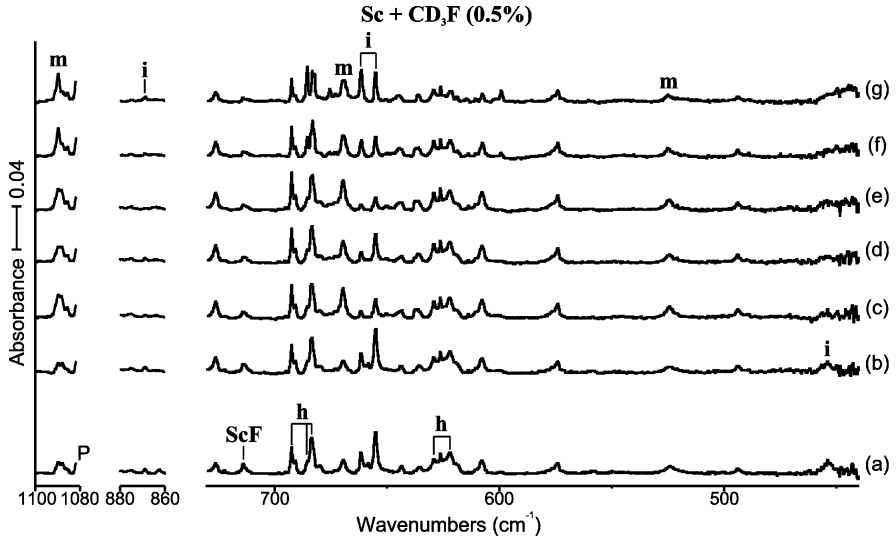

Figure 2. IR spectra in the regions of 1080−1100, 860−880, and 440−710 cm^{-1} for laser-ablated Sc atoms co-deposited with CD_3F in excess argon at 8 K. (a) Sc + 0.5% CD_3F in Ar co-deposited for 1 h. (b) After broad-band photolysis with a filter ($\lambda > 420$ nm). (c) After broad-band photolysis with a filter ($240 < \lambda < 380$ nm). (d) After broad-band photolysis with a filter ($\lambda > 420$ nm). (e) After broad-band photolysis with a filter ($240 < \lambda < 380$ nm). (f) After annealing to 28 K. (g) After annealing to 36 K. **i**, **m**, and **h** denote the product absorption group, and P indicates precursor absorption.

TABLE 1: Frequencies of Product Absorptions Observed from Reactions of CH_3X with Sc in Excess Argon[a]

	CH_3F	CD_3F	$^{13}CH_3F$	CH_3Cl	CD_3Cl	CH_3Br	description
i	1106.9	868.9	1097.7				CH_3 deform
	656.7	655.2	656.4				Sc−X str
	505.9	453.8	496.5				C−Sc str
m	1511.2	**1089.7**, 1087.7	1511.3	1524.8	1092.9	1527.9	Sc−H str
	679.5	669.6	679.0				Sc−X str
	565.3		553.9	586.1			CH_2 wag
	481.2		472.4				CScH bend
h	696.2, 687.3	692.3, 683.3	696.0, 686.8				Sc−F str
	630.9, 625.1	629.0, 621.9	630.4, 625.0				Sc−F str

[a] All frequencies are in cm^{-1}. A stronger absorption is bold. Description gives major coordinate. **i**, **m**, and **h** stand for the insertion, methylidene, and high-order products, respectively.

and Sc−D stretching frequencies are compared with the hydrogen stretching frequencies of ScH, ScH_3, ScD, and ScD_3 at 1530.4, 1487.8, 1103.4, and 1079.1 cm^{-1}, respectively.[28] The strong Sc−H absorption suggests that the product responsible for the **m** absorptions has an Sc−H bond. There is no **i** absorption in the Sc−H stretching frequency region.

Group 4−6 metals react with CH_4 and CH_3X to form the insertion and higher oxidation state products (CH_3-MX, $CH_2{=}MHX$, and $CH{\equiv}MH_2X$, X = H or halogen).[15] Group 3 metals also activate methane to CH_3-MH and CH_2-MH_2.[17] On the basis of the previous results[15,17] and new bands in the Sc−H stretching region, the energetically most plausible reaction product responsible for the **i** absorptions is a Grignard-type species,[1] CH_3-ScF, while that for the **m** absorptions is CH_2-ScHF. It will be shown below that the other absorptions in the low-frequency region also support these identifications.

Another strong **m** absorption is observed at 679.5 cm^{-1}, and its D and ^{13}C counterparts are seen at 669.6 and 679.0 cm^{-1} (H/D and $^{12}C/^{13}C$ ratios of 1.015 and 1.001), respectively. The small isotopic shifts indicate that the band originates from a vibrational mode that does not include large displacements of hydrogen or carbon atoms. This frequency is compared with the ScF, ScF_2, and ScF_3 frequencies of 735.6, 685.0, and 692.0 cm^{-1}.[29−32] The absorption is assigned to the Sc−F stretching mode of CH_2-ScHF. On the red side of the **m** absorption, an **i** absorption, which is strongest among the **i** absorptions, is observed at 656.7 cm^{-1}. The D and ^{13}C counterparts are observed at 655.2 and 656.4 cm^{-1} (the H/D and $^{12}C/^{13}C$ ratios of 1.002 and 1.000), respectively. On the basis of the strong intensity and the small isotopic ratios, the band is assigned to the Sc−F stretching absorption of CH_3-ScF.

The **m** absorption at 565.3 cm^{-1} has its ^{13}C counterpart at 553.9 cm^{-1} ($^{12}C/^{13}C$ ratio of 1.021), while the D counterpart is not observed probably due to its low frequency. The band is assigned to the CH_2 wagging mode. Another **m** absorption at 481.2 cm^{-1} and its ^{13}C counterpart at 472.4 cm^{-1} ($^{12}C/^{13}C$ ratio of 1.018) are attributed to the CScH bending mode. The **i** absorption at 505.9 cm^{-1} has D and ^{13}C shifts of −52.1 and −9.4 cm^{-1} (H/D and $^{12}C/^{13}C$ ratios of 1.115 and 1.019), and on account of the frequency and isotopic shifts, the band is assigned to the C−Sc stretching mode. A weak **i** absorption is observed at 1106.9 cm^{-1} and its D and ^{13}C counterparts at 868.9 and 1097.7 cm^{-1} (H/D and $^{12}C/^{13}C$ ratios of 1.274 and 1.008), respectively. On the basis of the frequency and the large H/D ratio, it is assigned to the CH_3 deformation mode.

As described above, the observed **i** and **m** absorptions and their variations show that scandium also forms the insertion product (CH_3-ScF) in the reaction with methyl fluoride and the methylidene complex (CH_2-ScHF) via following α-hydrogen migration. Hydrogen migration is apparently reversible, resulting in the interchange between CH_3-ScF and CH_2-ScHF as shown in Figure 1 and Scheme 1. The present results show that reaction of metal atoms with small organic molecules and following photolysis is an effective method to provide the rarely studied group 3 metal methylidenes.

SCHEME 1

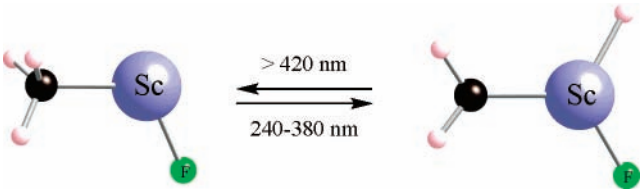

The calculated harmonic frequencies for CH_3-ScF and CH_2-ScHF listed in Tables 2 and 3 are in the range of agreement expected for the B3LYP density functional with the observed values. A footnote comparison shows that the ultrafine grid makes little difference in the computed frequencies. Similar calculations with the BPW91 functional gave comparable frequencies (Table S1 of the Supporting Information).

The anharmonic frequencies[24] show much better agreement (within 1% especially for the high-frequency stretching modes), parallel to the previous products from Sc and CH_4.[17] However, the anharmonic calculation often overcorrects for low-frequency modes (e.g., the CScH bending mode of CH_2-ScHF), and the predicted anharmonic frequency for the low-frequency CH_3 distortion of the insertion complex is an unreasonable imaginary value. The anharmonic frequency calculation is particularly susceptible to the condition of the potential energy surface because it depends on the numerical differentiation of the surface. It is difficult to model the shallow bending potentials for the bending and deformation frequencies.

The Sc−F stretching frequency region in Figures 1 and 2 contains absorptions marked **h**. In the previous study of group 3 metals + CH_4, broad absorption features in the hydrogen stretching region are also attributed to higher-order products, but the structures are not identified.[17] The relatively small increase of the higher-order product on annealing as shown in Figures 1 and 2 suggests that conversion to the higher-order product requires activation energy.

Extensive calculations were carried out in an effort to identify the higher-order product, and the most energetically plausible are $(CH_3)_2ScF_2$ and CH_3ScF_2. $(CH_3)_2ScF_2$ particularly draws attention because analogous higher-order products ($(CH_3)_2MX_2$, X = H or halogen) have been identified from reactions of group 4 and 5 metals with CH_4 and CH_3X.[15] McGrady et al. also synthesized $(CH_3)_2TiCl_2$ from reaction of $TiCl_4$ with $(CH_3)_2Zn$,[33] and its matrix frequencies are consistent with the observed values for the higher-order product in the Ti + CH_3Cl spectra.[9b] The absorptions of the higher-order products of group 4 and 5 metals, however, increase dramatically in the process of annealing as well as at high reagent concentrations.

While the calculated structure of $(CH_3)_2ScF_2$ is similar to the analogous products for group 4 and 5 metals,[15] the vibrational characteristics are not. Especially a strong antisymmetric CH_3 deformation band would appear at around 800 cm^{-1}, which is not observed in the Sc + CH_3F spectra. In contrast, the CH_3-ScF_2 molecule basically reproduces the observed vibrational characteristics of the **h** absorptions. The only strong bands of CH_3-ScF_2 arise from the Sc−F stretching modes, which are about 30 cm^{-1} higher and lower than that for CH_3-ScF.

The fact that the higher-order product is produced almost exclusively during deposition suggests that metal atoms with excess energy are needed to form the product. The Sc atom in fact can extract the F atom from CH_3F to form ScF, reaction 1. ScF then can undergo a reaction with CH_3F to form the final product, reaction 2, and the reaction exothermicity is actually higher than that of Sc + CH_3F, reaction 3. Siegbahn et al. investigated theoretically methane activation by second-row transition-metal halides and show that they are as effective as the metal atoms.[5]

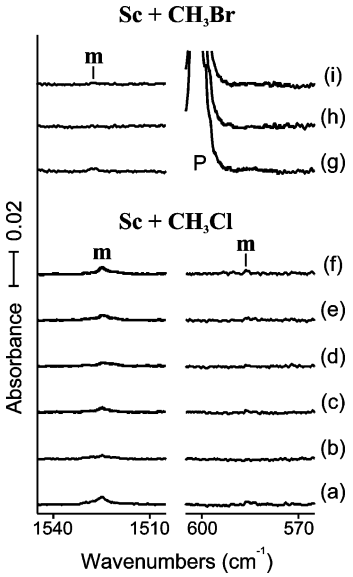

Figure 3. IR spectra in the regions of 1505−1545 and 565−605 cm^{-1} for laser-ablated Sc atoms co-deposited with CH_3Cl (a−f) and CH_3Br (g−i) in excess argon at 8 K. (a) Sc + 0.2% CH_3Cl in Ar co-deposited for 1 h. (b) After broad-band photolysis with a filter (λ > 420 nm). (c) After broad-band photolysis with a filter (240 < λ < 380 nm). (d) After broad-band photolysis with a filter (λ > 420 nm). (e) After broad-band photolysis with a filter (240 < λ < 380 nm). (f) After annealing to 28 K. (g) Sc + 0.2% CH_3Br in Ar co-deposited for 1 h. (h) After broad-band photolysis with a filter (λ > 420 nm). (i) After broad-band photolysis with a filter (240 < λ < 380 nm). **m** denotes the product absorption group.

$$Sc + CH_3F \rightarrow ScF + CH_3. \quad -36 \text{ kcal/mol} \quad (1)$$

$$ScF + CH_3F \rightarrow CH_3ScF_2 \quad -106 \text{ kcal/mol} \quad (2)$$

Another possible reaction path to CH_3-ScF_2 is to abstract a

$$Sc + CH_3F \rightarrow CH_3ScF \quad -94 \text{ kcal/mol} \quad (3)$$

fluorine atom from CH_3F by CH_3-ScF, reaction 4, which would release 47 kcal/mol, comparable with 56 kcal/mol released by formation of $(CH_3)_2ScF$ from CH_3ScF and CH_3F, reaction 5.

$$CH_3ScF + CH_3F \rightarrow CH_3-ScF_2 + CH_3. \quad -47 \text{ kcal/mol} \quad (4)$$

$$CH_3ScF + CH_3F \rightarrow (CH_3)_2ScF_2 \quad -56 \text{ kcal/mol} \quad (5)$$

Either way, formation of CH_3-ScF_2 is highly feasible, and more evidence is necessary to confidently identify the product responsible for the **h** absorptions. Observation of the ScF absorption would support formation of CH_3-ScF_2. The gas-phase frequency of ScF is known (735.6 cm^{-1}),[29,30] and the neon matrix fundamental has been assigned as 720 cm^{-1}.[31] Hence, the 714.1 cm^{-1} band observed in both the Sc + CH_3F and Sc + CD_3F spectra is assigned to ScF in solid argon. The CH_3 absorption may be hidden by the **h** band near 615 cm^{-1}, and CD_3 is in fact observed as part of the absorption at 453 cm^{-1}.[14]

The reactions of Sc with CH_3Cl and CH_3Br were also done, and the IR spectra are illustrated in Figure 3. Previous studies show that CH_3Cl and CH_3Br are as reactive as CH_3F with early transition metals.[15] Formation of the Sc insertion complexes

TABLE 2: Calculated Frequencies of CH_3-ScX Isotopomers in the Ground $^2A'$ Electronic State[a]

	CH_3-ScF			CD_3-ScF		$^{13}CH_3-ScF$		CH_3-ScCl			CD_3-ScCl		CH_3-ScBr			CD_3-ScBr	
approx description	anharm.[b]	harm.	int	harm.	int.	harm.	int	anharm.[b]	harm.	int	harm.	int	anharm.[b]	harm.	int	harm.	int
A′ CH_3 str	2912.8	3079.8	9	2275.4	3	3069.4	9	2916.4	3077.9	6	2273.3	2	2912 .5	3076.3	6	2272.0	2
A′ CH_3 str	2822.8	2974.8	6	2133.3	1	2971.6	6	2939.4	2972.7	6	2132.1	2	2833 .9	2972.0	7	2131.7	2
A′ CH_3 bend	1374.5	1419.9	0	1030.0	0	1416.8	0	1368.8	1415.7	0	1027.3	0	1362.4	1415.2	0	1027.0	0
A′ CH_3 deform	1105.5	1139.0	11	891.9	26	1130.0	9	1103.8	1139.8	11	893.6	27	1107.4	1140.3	10	894.0	27
A′ Sc-X str	654.8	667.8	17 1	666.2	167	667.7	17 1	410.3	429.4	10 2	405.5	91	277.1	289.8	37	264.0	9
A′ C-Sc str	464.8	510.3	65	458.1	63	500.8	61	492.1	504.4	82	458.6	85	485.6	501.5	82	454.1	77
A′ CH_3 rock	438.4	414.8	21	325.6	7	410.4	23	336.5	358.5	18	290.1	4	334.5	396.1	54	331.7	64
A′ CScX bend	99.4	133.2	6	123.8	5	132.2	5	89.9	98.9	4	90.9	3	61.9	88.3	2	80.4	2
A″ CH_3 str	2895.1	3038.7	7	2245.1	2	3028.2	7	2873.4	3036.5	8	2243.3	2	2875.5	3035.8	8	2242.8	2
A″ CH_3 bend	1369.0	1430.1	10	1038.1	7	1426.9	10	1378.2	1428.4	10	1036.5	7	1379.6	1427.8	10	1036.0	7
A″ CH_3 rock	344.8	379.7	7	283.9	5	377.8	6	349.7	371.4	9	277.8	7	345.9	369.7	10	276.4	8
A″ CH_3 distort	−3714.5	4.2	1	7.1	2	4.2	1	−62.4	49.4	1	34.9	1	−124.0	52.9	0	37.5	1

[a] Harmonic frequencies and intensities computed with B3LYP/6-311++G(3df,3pd), and the all-electron basis is used for Sc. Frequencies and intensities are in cm^{-1} and km/mol. Ultrafine grid used for CH_3-ScF. [b] Anharmonic frequencies.

TABLE 3: Calculate Frequencies of CH_2-ScHX Isotopomers in the Ground $^2A''$ Electronic State[a]

	CH_2-ScHF			CD_2-ScDF		$^{13}C\ H_2-ScHF$		$CH_2-ScHCl$			$CD_2-ScDCl$		$CH_2-ScHBr$			$CD_2-ScDBr$	
approx description	anharm.[b]	harm.	int	harm.	int	harm.	int	anharm.[b]	harm.	int	harm.	in.	anharm.[b]	harm.	int	harm.	int
A′ CH str	2947.6	3109.8	13	2302.5	4	3098.4	14	2955.7	3114.4	10	2306.0	3	2952.7	3115.4	9	2306.8	3
A′ CH str	2886.9	3033.0	8	2200.8	1	3027.1	9	2891.7	3035.2	6	2202.3	0	2888.8	3035.9	5	2202.7	0
A′ Sc−H str	1491.1	1551.3	511	1109.9	28 0	1551.3	511	1529.3	1571.3	517	1124.0	279	1518.3	1575.3	527	1126.8	284
A′ CH_2 sciss	1359.3	1369.2	2	1023.0	10	1363.4	2	1354.3	1363.1	2	1019.9	10	1351.0	1360.9	2	1018.7	11
A′ Sc−X str	688.7	699.3	326	683.3	245	698.7	323	381.9	380.4	25	337.3	2	288.6	292.4	25	275.7	12
A′ C−Sc str	565.0	572.1	99	532.2	83	561.1	101	593.7	599.8	258	549.6	173	585.0	594.6	227	545.9	150
A′ CScH bend	474.6	492.6	19	379.0	24	489.2	18	508.7	518.2	53	444.0	89	489.7	509.1	41	407.9	63
A′ CH_2 rock	355.8	375.0	9	288.7	11	372.2	8	343.3	354.6	9	266.5	8	329.3	349.8	7	261.2	7
A′ CScX bend	139.4	145.1	2	131.9	2	144.1	2	108.3	110.5	2	100.6	2	94.6	97.2	2	87.9	1
A″ CH_2 wag	596.5	609.6	82	478.1	63	604.3	79	581.0	612.8	77	480.7	58	583.7	612.0	75	480.1	56
A″ CH_2 twist	203.6	209.6	36	148.7	16	209.5	36	211.9	198.3	66	140.7	37	183.8	198.2	86	140.9	50
A″ ScH OOP bend	80.3	99.7	290	75.6	174	99.6	290	233.9	102.8	201.3	80.0	115	114.5	110.2	164	83.0	90

[a] Harmonic frequencies and intensities computed with B3LYP/6-311++G(3df,3pd), and all-electron basis is used for Sc. Frequencies and intensities are in cm^{-1} and km/mol. CH_2-ScHF has also a C_s (planar) structure at other levels of theory (BPW91, MP2, and CCSD). The symmetry notations are based on the C_s structure. [b] Anharmonic frequencies. All frequencies in table calculated using fine grid: in contrast, the frequencies in the third, tenth, and twelfth rows of columns one and two are 1501.9, 1549.7, 591.8, 609.5, 81.2, and 101.6 cm^{-1} using ultrafine grid.

from CH_3Cl and CH_3Br are both energetically favorable, reactions 6 and 7.

$$Sc + CH_3Cl \rightarrow CH_3ScCl \qquad -86\ \text{kcal/mol} \qquad (6)$$

$$Sc + CH_3Br \rightarrow CH_3-ScBr \qquad -79\ \text{kcal/mol} \qquad (7)$$

However, the product absorptions in Figure 3 are clearly far weaker than those in the Sc + CH_3F spectra, and the weak absorptions become even weaker in the process of photolysis. This suggests that the Sc reaction products easily dissociate by laser plume radiation. The 1524.8 cm^{-1} band with CH_3Cl shifts to 1092.9 cm^{-1} with CD_3Cl (H/D ratio 1.3952), which is appropriate for the Sc−H stretching mode in the $CH_2-ScHCl$ complex. Furthermore the CH_2 wag at 586.1 is just slightly higher than this mode for CH_2-ScHF.

It is also interesting that the Sc−H bond length decreases and the Sc−H stretching frequency increases with increasing halogen size in the CH_2-ScHX complexes. The Sc−H stretching frequency increases by 13.6 cm^{-1} on substitution of F with Cl, and it further increases by 3.1 cm^{-1} on substitution of Cl with Br. Similar trends are also reported in previous investigations with early transition metals.[9,10] The lower electronegativity of the larger halogen is expected to allow more electron density to remain in the Sc−H bond, resulting in a stronger Sc−H bond and the higher stretching frequency. This is also manifest in a shorter C−Sc bond.

Y + CH_3X. Figures 4 and 5 show that the IR spectra from reactions of laser-ablated Y atoms with CH_3F and CD_3F. Parallel to the Sc case, three sets of product absorptions are marked **i**, **m**, and **h** on the basis of the behaviors upon photolysis and annealing, and the observed frequencies are summarized in Table 4. Both the **i** and **m** absorptions in the original spectra after deposition show almost no change on visible irradiation, but the **i** absorptions disappear completely upon UV irradiation, while the **m** absorptions almost triple. This suggests that the product responsible for **i** absorptions converts upon UV irradiation to another product responsible for the **m** absorptions. The absorptions marked **h** are less visible relative to those in the Sc + CH_3F spectra in Figures 1 and 2. They remain virtually unchanged in the process of photolysis and annealing but increase considerably at high concentration, similar to those in the Sc + CH_3F spectra. Also shown is a weak absorption for OYO^- from target surface impurity.[34]

The most distinctive product absorption is the **m** absorption at 1397.7 cm^{-1} in Figure 4, which shows no ^{13}C shift but a sizable D shift of −397.2 cm^{-1} (H/D ratio of 1.397). The frequency is compared with the Y−H and Y−D stretching frequencies of 1385.1 and 995.4 cm^{-1} for YH_3 and YD_3,[28] although no absorptions of binary yttrium hydrides are observed. The single strong product Y−H stretching absorption indicate that parallel to the Sc + CH_3F case, the Y methylidene complex (CH_2-YHF) is formed during deposition and UV photolysis afterward. No **i** absorptions are observed in the Y−H stretching region, and therefore, the **i** absorptions most probably originate from the insertion complex (CH_3-YF), which is energetically most plausible.

Another strong **m** absorption is observed at 575.1 cm^{-1}, and its D and ^{13}C counterparts are seen at 567.3 and 575.3 cm^{-1},

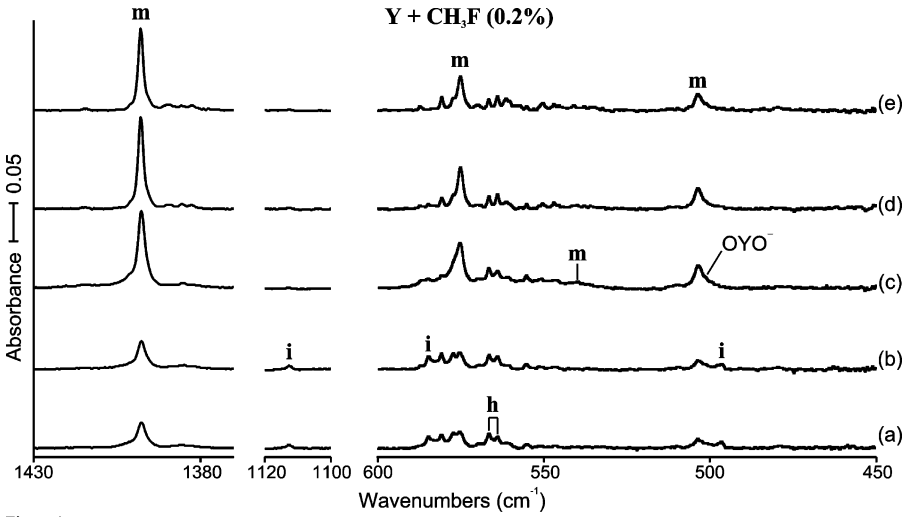

Figure 4. IR spectra in the regions of 1370−1430, 1100−1120, and 550−830 cm^{-1} for laser-ablated Y atoms co-deposited with CH_3F in excess argon at 8 K. (a) Y + 0.2% CH_3F in Ar co-deposited for 1 h. (b) After broad-band photolysis with a filter (λ > 420 nm). (c) After broad-band photolysis with a filter (240 < λ < 380 nm). (d) After annealing to 28 K. (e) After annealing to 36 K. **i** and **m** denote the product absorption group.

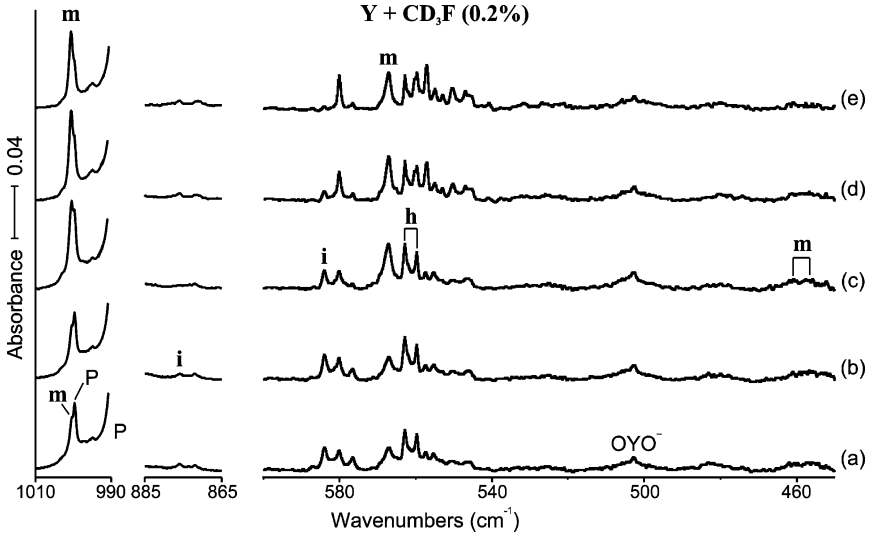

Figure 5. IR spectra in the regions of 990−1010, 865−885, and 450−600 cm^{-1} for laser-ablated Y atoms co-deposited with CD_3F in excess argon at 8 K. (a) Y + 0.2% CD_3F in Ar co-deposited for 1 h. (b) After broad-band photolysis with a filter (λ > 420 nm). (c) After broad-band photolysis with a filter (240 < λ < 380 nm). (d) After annealing to 28 K. (e) After annealing to 36 K. **i**, **m**, and **h** denote the product absorption groups, and P stands for precursor absorption.

TABLE 4: Frequencies of Product Absorptions Observed from Reactions of CH_3X with Y in Excess Argon[a]

	CH_3F	CD_3F	$^{13}CH_3F$	CH_3Cl	CD_3Cl	CH_3Br	CD_3Br	description
i	1112.7	875.9	1104.4	1113.7		1111.7		CH_3 deform
	584.7	584.0	584.4					Y−X str
	496.5			459.7				C−Y str
m	1397.7	1000.5	1397.7	1419.6	1018.6	1424.3	1021.2	Y−H str
	575.1	567.3	575.3					Y−X str
	540.0	457.4	527.6					CH_2 wag
	503.5	461.0	493.4	510.1	466.2	509.7	466.2	C−Y str
				454.7				CYH bend
h	566.6, 563.9	562.9, 559.8	566.2, 563.7					Y−F str

[a] All frequencies are in cm^{-1}. Description gives major coordinate. **i**, **m**, and **h** stand for insertion, methylidene, and high-order products, respectively.

which are compared with the previously reported YF, YF_2, and YF_3 frequencies of 631.29, 550, and 663 cm^{-1}, respectively.[29,31,35] On the basis of the frequencies and small isotopic shifts, they are assigned to the Y−F stretching mode. A weak **m** absorption emerges at 540.0 cm^{-1}, and its D and ^{13}C counterparts emerge at 457.4 and 527.6 cm^{-1} (H/D and $^{12}C/^{13}C$ ratios of 1.180 and 1.024). They are assigned to the CH_2 wagging mode. Another sizable **m** absorption at 503.5 cm^{-1} and its D and ^{13}C counterparts at 461.0 and 493.4 cm^{-1} (H/D and $^{12}C/^{13}C$ ratios of 1.092 and 1.020) are attributed to the C−Y stretching mode on the basis of the frequencies and isotopic shifts. The **i** absorptions are much weaker relative to the Sc + CH_3F case. The **i** absorption at 1112.7 cm^{-1} has its D and ^{13}C counterparts at 875.9 and 1104.4 cm^{-1} (H/D and $^{12}C/^{13}C$ ratios of 1.270 and 1.008) and is attributed to the CH_3 deformation mode. On the blue side of the Y−F stretching absorption of

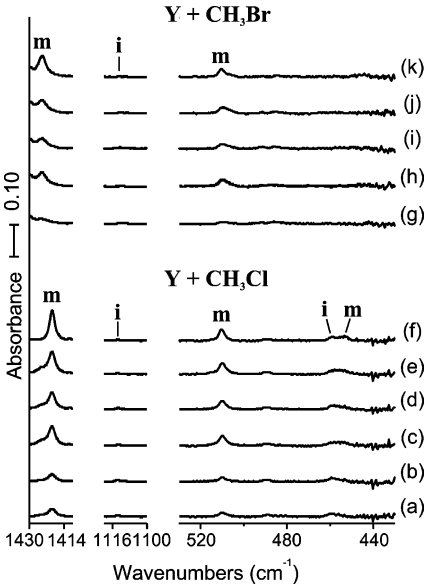

Figure 6. IR spectra in the regions of 1410−1430, 1100−1120, and 430−530 cm^{-1} for laser-ablated Y atoms co-deposited with CH_3Cl (a−f) and CH_3Br (g−k) in excess argon at 8 K. (a) Y + 0.2% CH_3Cl in Ar co-deposited for 1 h. (b) After broad-band photolysis with a filter (λ > 420 nm). (c) After broad-band photolysis with a filter (240 < λ < 380 nm). (d) After broad-band photolysis with a filter (λ > 420 nm). (e) After broad-band photolysis with a filter (240 < λ < 380 nm). (f) After annealing to 28 K. (g) Y + 0.2% CH_3Br in Ar co-deposited for 1 h. (h) After broad-band photolysis with a filter (240 < λ < 380 nm). (i) After broad-band photolysis with a filter (λ > 420 nm). (j) After broad-band photolysis with a filter (240 < λ < 380 nm). (k) After annealing to 28 K. **i** and **m** denote the product absorption groups.

CH_2−YHF, an **i** absorption is observed at 584.7 cm^{-1} and shows very small D and ^{13}C shifts of 0.7 and 0.3 cm^{-1}. It is assigned to the Y−F stretching mode of CH_3−YF. The **i** absorption at 496.5 cm^{-1} without observation of its D and ^{13}C counterparts is attributed to the C−Y stretching mode. The observed vibrational characteristics support formation of CH_3−YF.

Parallel to the case of Sc + CH_3F, the observed **h** absorptions are believed to be due to the Y−F stretching bands of a high-order product mostly formed during deposition. The invariance of the intensities in the process of photolysis and annealing indicates that only the laser-ablated metal atoms can undergo the reaction to form the high-order product. $(CH_3)_2YF_2$ and CH_3-YF_2 are considered as plausible products, parallel to the Sc case. $(CH_3)_2YF_2$ would give not only the Y−F stretching absorptions but a strong asymmetric CH_3 deformation absorption ∼ 750 cm^{-1}, which is not observed in this study. On the other hand, the only strong enough absorptions of CH_3−YF_2 to observe are the symmetric and antisymmetric Y−F stretching absorptions.

Abstraction of the F atom from CH_3F by the laser-ablated Y atom is energetically favorable, parallel to the case of Sc + CH_3F, and the YF so produced can react with another CH_3F to form CH_3−YF_2, reactions 8 and 9. The reaction energy of YF + CH_3F is comparable to that of Y + CH_3F, reaction 10.

$$CH_3F + Y \rightarrow YF + CH_3. \qquad -48 \text{ kcal/mol} \qquad (8)$$

$$YF + CH_3F \rightarrow CH_3YF_2 \qquad -93 \text{ kcal/mol} \qquad (9)$$

$$Y + CH_3F \rightarrow CH_3YF \qquad -99 \text{ kcal/mol} \qquad (10)$$

Observation of the YF absorption would support the reaction path, but unfortunately the matrix YF frequency is not known. While the observed vibrational characteristics of the **h** absorptions and the variations upon photolysis and annealing favor formation of CH_3−YF_2 over $(CH_3)_2YF_2$, a definitive identification of the higher-order product will require more evidence.

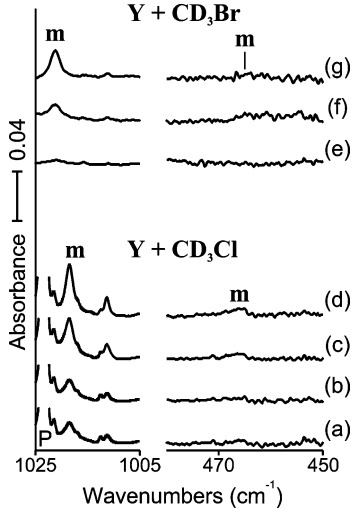

Figure 7. IR spectra in the regions of 1005−1025 and 450−480 cm^{-1} for laser-ablated Y atoms co-deposited with CD_3Cl (a−d) and CD_3Br (e−g) in excess argon at 8 K. (a) Y + 0.2% CD_3Cl in Ar co-deposited for 1 h. (b) After broad-band photolysis with a filter (λ > 420 nm). (c) After broad-band photolysis with a filter (240 < λ < 380 nm). (d) After annealing to 28 K. (e) Y + 0.2% CD_3Br in Ar co-deposited for 1 h. (f) After broad-band photolysis with a filter (240 < λ < 380 nm). (g) After annealing to 28 K.

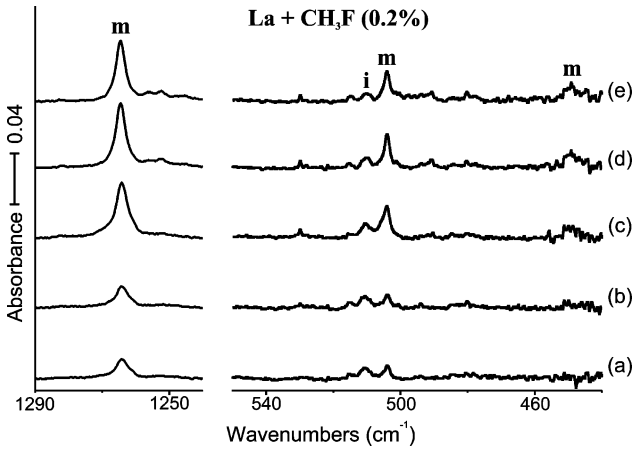

Figure 8. IR spectra in the regions of 1240−1290, and 440−550 cm^{-1} for laser-ablated La atoms co-deposited with CH_3F in excess argon at 8 K. (a) La + 0.2% CH_3F in Ar co-deposited for 1 h. (b) After broad-band photolysis with a filter (λ > 420 nm). (c) After broad-band photolysis with a filter (240 < λ < 380 nm). (d) After annealing to 28 K. (e) After annealing to 36 K.

The IR spectra from reactions of Y with CH_3Cl and CH_3Br are also shown in Figures 6 and 7, and the measured product frequencies are listed in Table 4. Unlike the case of Sc, the product absorptions are quite strong in the CH_3Cl and CH_3Br spectra. No **h** absorptions are observed, partly due to the low Y−Cl and Y−Br stretching frequencies. The Y−H stretching frequency of CH_2−YHX increases with increasing size of halogen, being consistent with the Sc case. Substitution of F with Cl increases the frequency by 21.9 cm^{-1}, whereas substitution of Cl with Br leads to an increase of 4.7 cm^{-1}. Table 4 also shows that the comparable C−Y stretching frequencies of 510.1 and 509.7 cm^{-1} for CH_2−YHCl and CH_2−YHBr are substantially higher than that of 503.5 cm^{-1} for CH_2−YHF. These results, consistent with the Sc case, are explained with the lower electronegativity of larger halogens, leaving more

TABLE 5: Calculated Frequencies of CH_3-YX Isotopomers in the Ground $^2A'$ Electronic State[a]

	CH_3-YF			CD_3-YF		$^{13}C\,H_3-YF$		CH_3-YCl			CD_3-YCl		CH_3-YBr			CD_3-YBr	
approx description	anharm.[b]	harm.	int	harm.	int	harm.	int	anharm,[b]	harm.	int	harm.	int	anharm.[b]	harm.	int	harm.	int
A′ CH_3 str	2874.5	3067.7	12	2265.5	4	3057.5	13	2921.5	3068.0	8	2265.4	3	2898.4	3069.7	7	2266.3	3
A′ CH_3 str	2818.8	2963.9	11	2126.8	2	2960.5	11	2829.3	2963.6	9	2126.7	2	2892.0	2961.2	9	2125.4	2
A′ CH_3 bend	1381.6	1422.2	0	1031.4	0	1419.1	0	1365.5	1417.6	0	1028.3	0	1471.2	1416.2	0	1027.4	0
A′ CH_3 deform	1121.1	1141.7	15	888.1	24	1133.1	13	1118.9	1143.7	17	891.0	28	1123.4	1144.8	18	892.2	29
A′ Y−X str	583.1	592.4	11 0	591.3	11 0	592.3	11 1	337.0	335.1	32	349.3	67	247.4	242.3	28	236.9	18
A′ C−Y str	427.8	465.9	38	412.4	37	457.3	33	458.2	464.4	40	414.1	38	412.2	465.7	44	415.6	41
A′ CH_3 rock	511.4	397.6	15	313.6	5	391.9	17	386.0	384.5	47	285.8	0	608.9	372.3	26	293.8	24
A′ CYX bend	99.3	113.8	6	106.1	6	112.8	6	98.7	84.8	3	78.2	3	250.1	76.2	2	68.9	2
A″ CH_3 str	2890.8	3022.9	8	2232.6	3	3012.6	8	2853.8	3023.3	7	2232.9	2	2967.0	3020.1	7	2230.4	2
A″ CH_3 bend	1358.5	1431.9	10	1039.4	7	1428.7	10	1393.1	1428.7	10	1036.9	7	1411.6	1428.4	10	1036.6	7
A″ CH_3 rock	298.6	358.8	2	267.3	2	357.0	2	325.2	353.1	2	263.1	2	435.4	348.0	2	259.4	2
A″ CH_3 distort	−6428.4	2.5	0	6.5	1	2.5	0	−95.8	24.7	0	18.8	0	20402.7	5.0	0	7.3	0

[a] Harmonic frequencies and intensities computed with B3LYP/6-311++G(3df,3pd), and SDD core potential and basis set are used for Y. Frequencies and intensities are in cm^{-1} and km/mol. [b] Anharmonic frequencies.

TABLE 6: Calculated Fundamental Frequencies of CH_2-YHX Isotopomers in the Ground ^2A Electronic State[a]

	CH_2-YHF			CD_2-YDF		$^{13}CH_2-YHF$		CH_2-YHCl			CD_2-YDCl		CH_2-YHBr			CD_2-YDBr	
approx description	anharm.[b]	harm.	int	harm.	int	harm.	int	anharm.[b]	harm.	int	harm.	int	anharm.[b]	harm.	int	harm.	int
CH str	2928.4	3094.6	19	2290.4	6	3083.3	19	2933.5	3097.6	15	2292.6	5	2934.1	3098.5	14	2293.2	5
CH str	2877.0	3023.9	18	2194.2	3	3018.0	20	2879.5	3025.8	14	2195.7	2	2881.1	3025.9	14	2195.8	2
Y−H str	1399.3	1445.5	494	1029.3	240	1445.5	494	1428.7	1465.9	531	1043.1	27 7	1441.7	1467.6	552	1044.2	288
CH_2 sciss	1361.3	1375.1	3	1022.2	25	1369.7	3	1361.5	1375.3	1	1023.7	7	1358.0	1373.9	1	1022.7	7
Y−X str	590.5	595.9	254	585.5	187	595.4	257	321.8	327.8	32	311.9	10	233.1	235.0	23	229.1	15
CH_2 wag	565.0	587.3	82	458.2	57	582.4	74	571.2	597.2	70	466.2	57	571.4	596.3	69	465.8	53
C−Y str	502.7	507.3	131	468.7	94	496.7	134	524.5	526.2	246	475.4	12 7	489.6	526.7	229	475.3	124.6
CYH bend	445.6	455.8	20	351.6	32	451.4	16	467.4	478.0	34	389.2	94	439.2	476.9	23	374.7	55
CH_2 rock	338.3	356.0	20	269.2	20	353.8	18	323.3	344.2	20	254.8	12	290.2	338.1	12	252.0	14
CH_2 twist	171.8	196.4	47	140.1	24	196.4	47	176.3	198.7	36	140.8	18	126.9	199.4	57	141.1	29
CYX bend	48.0	143.1	116	115.6	28	142.5	119	121.0	104.8	47	91.2	13	81.5	83.8	2	75.7	2
YH OOP bend	15.5	83.2	162.5	71.0	128	82.4	159	−103.6	45.2	222	36.0	13 6	−498.8	80.6	243	55.7	134

[a] Harmonic frequencies and intensities computed with B3LYP/6-311++G(3df,3pd), and SDD core potential and basis set are used for Y. Frequencies and intensities are in cm^{-1} and km/mol. CH_2-YHF and CH_2-YHCl have C_1 structures, whereas CH_2-YHBr has a C_s (planar) structure with B3LYP and BPW91, whereas they all have C_s (planar) structures with MP2 and CCSD. [b] Calculated anharmonic frequencies.

TABLE 7: Frequencies of Product Absorptions Observed from Reactions of CH_3X with La in Excess Argon[a]

	CH_3F	CD_3F	$^{13}CH_3F$	CH_3Cl	CD_3Cl	description
i	510.4	510.2	510.4			La−X str
m	1264.2	904.5	1264.1	1291.0	923.1	La−H str
	529.8					CH_2 wag
	503.9	498.4	503.6			La−X str
	449.8		438.0	455.4		C−La str

[a] All frequencies are in cm^{-1}. Stronger absorptions are bold. Description gives major coordinate.

electron density in the Y−H and C−Y bonds.[15] Tables 5 and 6 summarize the B3LYP calculated harmonic frequencies for the CH_3-YX and CH_2-YHX molecules and such frequencies calculated with anharmonic correction, and again this correction is substantial only for the highest-frequency stretching modes. Table S2 (Supporting Information) compares harmonic frequencies calculated using the BPW91 functional.

La + CH_3X. The IR spectra from reactions of La with CH_3F are shown in Figures 8 and S1 (Supporting Information), and the frequencies are listed in Table 7. The absorptions marked **i** and **m** remain unchanged upon visible irradiation, but they increase about 40 and 300% upon UV irradiation, respectively. No **h** absorptions are observed, and apparently the yield for the higher-order product decreases with increasing atomic weight of the metal. The strong **m** absorption at 1264.2 cm^{-1} in the La−H stretching region shows no ^{13}C shift and a D shift of −359.7 cm^{-1} (H/D ratio of 1.398). The La−H stretching frequency is compared with that of 1263.6 cm^{-1} for LaH_3.[32,36] No absorptions of lanthanum hydrides are observed in this study. The single strong La−H absorption shows that CH_2-LaHF is readily formed in reaction of La with CH_3F and particularly on photolysis afterward.

Only one **i** absorption is observed at 510 cm^{-1}, as shown in Figure 8, and it has D and ^{13}C counterparts at 510.2 and 510.4 cm^{-1}. Deuteration leads to a relatively stronger **i** absorption, as shown in Figure 9, consistent with the previous cases of early transition-metal reactions with methane and methyl halides.[9−14,17] Deuteration evidently decreases the rate of α-hydrogen migration for conversion of CH_3-MX to CH_2-MHX. On the basis of the frequency and small isotopic shifts, the **i** band is attributed to the La−F stretching mode. The frequency is also compared with the LaF and LaF_2 ν_3 frequencies of 570 and 539 cm^{-1}, respectively.[29,36] While no other **i** absorptions are observed, we attribute the **i** absorption to the insertion complex (CH_3-LaF).

The strong **m** absorption at 503.9 cm^{-1} and its D and ^{13}C counterparts at 498.4 and 503.6 cm^{-1} are attributed to the La−F stretching mode of CH_2-LaHF. On the further low-frequency region, another **m** absorption is observed at 449.8 and its ^{13}C counterpart at 438.0 cm^{-1}. They are assigned to the C−La stretching mode without observation of the D counterpart. A weak absorption is observed at 529.8 cm^{-1}, which increases substantially like other **m** absorptions. It is, however, rather sharp unlike other **m** absorptions, and the D and ^{13}C counterparts

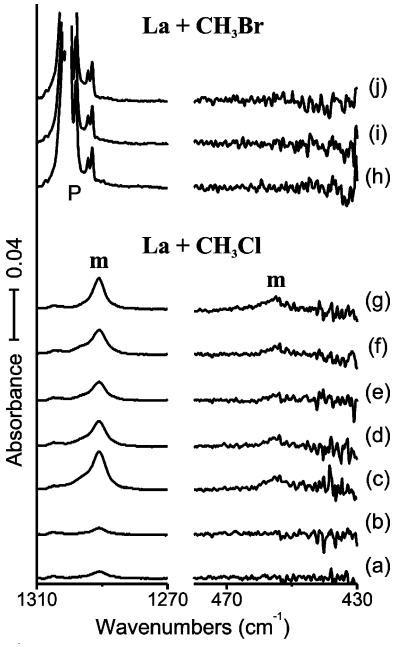

Figure 9. IR spectra in the regions of 1270−1310 and 430−480 cm^{-1} for laser-ablated La atoms co-deposited with CH_3Cl (a−g) and CH_3Br (h−j) in excess argon at 8 K. (a) La + 0.2% CH_3Cl in Ar co-deposited for 1 h. (b) After broad-band photolysis with a filter (λ > 420 nm). (c) After broad-band photolysis with a filter (240 < λ < 380 nm). (d) After broad-band photolysis with a filter (λ > 220 nm) for 10 min (e) After broad-band photolysis with a filter (λ > 420 nm). (f) After broad-band photolysis with a filter (240 < λ < 380 nm). (g) After annealing to 28 K. (h) La + 0.2% CH_3Br in Ar co-deposited for 1 h. (h) After broad-band photolysis with a filter (λ > 420 nm). (i) After broad-band photolysis with a filter (240 < λ < 380 nm). (j) After annealing to 28 K.

are not observed. The band is tentatively assigned to the CH_2 wagging mode of CH_2−LaHF.

The IR spectra from reactions of La with CH_3Cl and CH_3Br are shown in Figures 10 and S2 (Supporting Information). Absorptions with moderate intensities are observed in the CH_3Cl spectra, but none in the CH_3Br spectra. The reaction products of La with CH_3Br are apparently prone to dissociate. The **m** absorption halves on visible irradiation, but it increases dramatically (∼10 times) upon UV irradiation. The **m** absorptions exhibit photoreversible behavior as shown in Figure 10, unlike the La + CH_3F case, but the CH_3−LaCl participant could not be detected due to the low frequency of the three strongest modes.

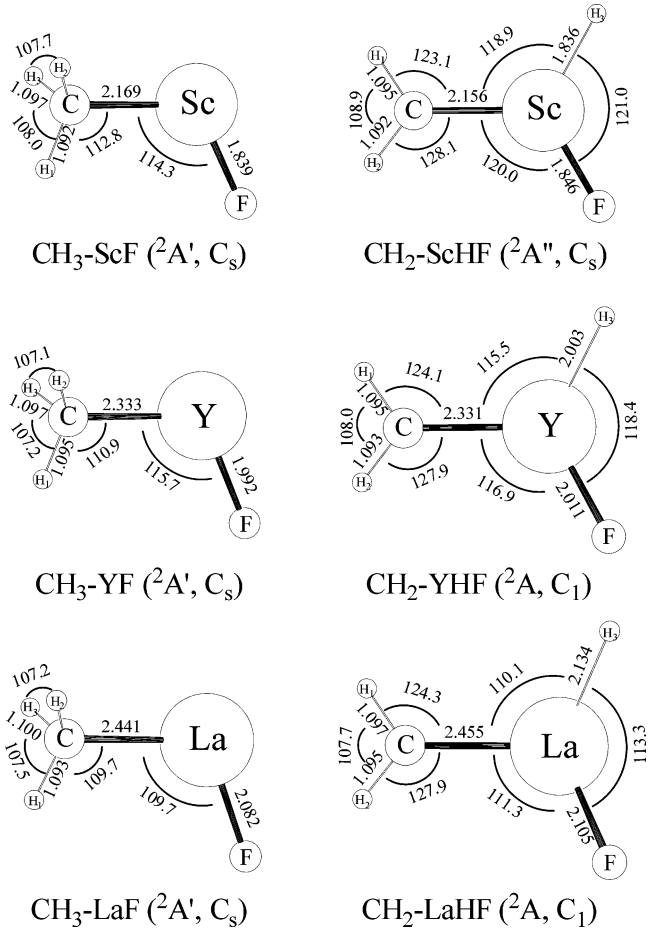

Figure 10. Optimized molecular structures of the insertion and methylidene complexes of group 3 metals with CH_3F calculated using B3LYP and the 6-311++G(3df,3pd) basis set. The all-electron basis is used for Sc, whereas the SDD pseudopotential and basis are used for Y and La. The bond lengths and angles are in angstroms and degrees. The electronic states and molecular symmetry are shown below the structure.

Substitution of F with Cl increases the La−H stretching frequency by 26.8 cm^{-1}, which is compared with 13.6 and 21.9 cm^{-1} for the Sc and Y methylidene complexes, respectively. This suggests that the effects of halogen size on the hydrogen stretching frequency become more important when going down the column. The C−La stretching frequency of 455.4 cm^{-1} is also 5.6 cm^{-1} higher than that of CH_2−LaHF. The low electronegativity of larger halogen leads to higher M−H and C−M stretching frequencies for all group 3 metal methylidene

TABLE 8: Calculated Frequencies of CH_3−LaX Isotopomers in the Ground $^2A'$ Electronic State[a]

	CH_3−LaF			CD_3−LaF		$^{13}CH_3$−LaF		CH_3−LaCl			CD_3−LaCl		CH_3−LaBr			CD_3−LaBr	
approx description	anharm.[b]	harm.	int	harm.	int	harm.	int	anharm.[b]	harm.	int	harm.	int	anharm.[b]	harm.	int	harm.	int
A′ CH_3 str	2921.5	3065.5	15	2263.5	6	3055.4	16	2926.9	3068.1	9	2265.2	4	2939.3	3068.4	8	2265.4	3
A′ CH_3 str	2822.5	2949.1	13	2116.0	3	2945.7	14	2801.2	2949.1	11	2116.1	3	2805.8	2949.1	10	2116.0	3
A′ CH_3 bend	1373.0	1415.2	0	1027.5	0	1411.9	0	1347.4	1411.9	0	1025.2	0	1383.9	1409.3	0	1023.5	0
A′ CH_3 deform	1102.8	1127.1	18	877.8	31	1118.3	15	1103.8	1132.6	19	883.8	34	1112.0	1131.2	20	883.1	36
A′ La−X str	523.8	534.2	13 0	533.0	132	533.9	130	295.7	302.5	38	308.9	79	213.8	210.8	32	207.3	22
A′ C−La str	405.0	416.6	69	368.0	60	407.8	63	419.7	423.3	64	375.2	54	435.9	420.9	69	373.7	59
A′ CH_3 rock	343.8	333.1	16	262.0	5	328.7	17	297.2	324.8	52	246.6	2	365.1	309.6	21	243.7	22
A′ CLaX bend	109.4	103.0	6	97.5	5	102.4	6	71.8	71.8	4	67.2	3	89.9	55.0	3	50.3	2
A″ CH_3 str	2853.4	3009.5	14	2223.2	5	2999.1	15	2826.0	3010.8	14	2224.4	5	2831.9	3011.4	14	2224.9	5
A″ CH_3 bend	1369.8	1427.5	13	1036.8	8	1424.1	12	1321.2	1424.6	12	1034.6	8	1391.3	1424.0	11	1034.1	7
A″ CH_3 rock	293.6	298.2	0	221.7	1	296.9	0	285.2	303.0	1	225.0	1	358.2	299.1	1	222.1	1
A″ CH_3 distort	218.9	26.6	0	23.6	1	26.6	0	−94.4	56.2	0	40.5	0	1633.8	32.4	0	24.2	0

[a] Harmonic frequencies and intensities computed with 6-311++G(3df,3pd), and SDD core potential and basis set are used for La. Intensities are calculated with B3LYP. Frequencies and intensities are in cm^{-1} and km/mol. [b] Calculated anharmonic frequencies.

TABLE 9: Calculated Frequencies of CH_2−LaHX Isotopomers in the Ground ^{2}A Electronic State[a]

	CH_2−LaHF			CD_2−LaDF		$^{13}CH_2$−LaHF		CH_2−LaHCl			CD_2−LaDCl		CH_2−LaHBr			CD_2−LaDBr	
approx description	anharm.[b]	harm.	int	harm.	int	harm.	Int	anharm.[b]	harm.	Int	harm.	Int	anharm.[b]	harm.	Int	harm.	int
CH str	2908.7	3073.9	26	2275.0	9	3062.7	27	2917.2	3082.2	19	2281.2	7	2927.5	3082.1	17	2281.3	7
CH str	2855.9	3001.4	29	2177.2	7	2995.6	31	2859.6	3005.7	22	2180.4	4	2860.7	3006.3	21	2180.7	4
CH_2 sciss	1335.6	1364.6	25	1014.2	4	1359.5	41	1277.0	1356.5	239	1013.3	5	1328.7	1363.5	245	1013.1	6
La−H str	1147.7	1336.0	696	949.8	363	1335.5	681	1218.6	1369.0	509	969.3	379	1293.7	1351	517	962.2	387
CH_2 wag	524.4	533.1	74	418.0	57	528.1	79	503.8	538.3	66	421.5	53	510.4	538.5	67	422.4	64
La−X str	507.6	524.0	231	520.3	191	523.7	226	274.7	293.2	41	281.9	15	220.1	209.0	73	203.0	26
C−La str	434.2	440.5	217	405.5	129	429.8	221	412.0	451.6	242	415.1	117	433.9	453.4	221	416.6	109.1
CLaH bend	352.4	399.1	45	301.7	51	395.9	34	329.3	428.0	86	334.2	148	390.4	421.9	71	319.7	79
CH_2 rock	251.7	319.4	34	242.8	28	317.5	33	230.9	308.1	47	229.1	15	275.6	292.5	18	218.6	24
LaH OOP bend	204.5	207.4	195	150.7	94	207.3	195	195.5	201.6	175	144.9	90	300.1	170.1	121	123.7	74
CH_2 twist	122.1	142.4	3	102.6	2	142.1	3	138.0	132.8	9	94.8	3	180.1	123.7	41	89.6	14
CLaX bend	94.9	101.0	30	94.4	25	100.3	29	77.1	71.5	18	64.9	16	93.9	65.1	22	58.4	19

[a] Harmonic frequencies and intensities computed with 6-311++G(3df,3pd), and SDD core potential and basis set are used for La. Frequencies and intensities are in cm^{-1} and km/mol. CH_2−LaHX has a C_1 structure at levels of B3LYP, BPW91, and MP2. [b] Calculated anharmonic frequencies.

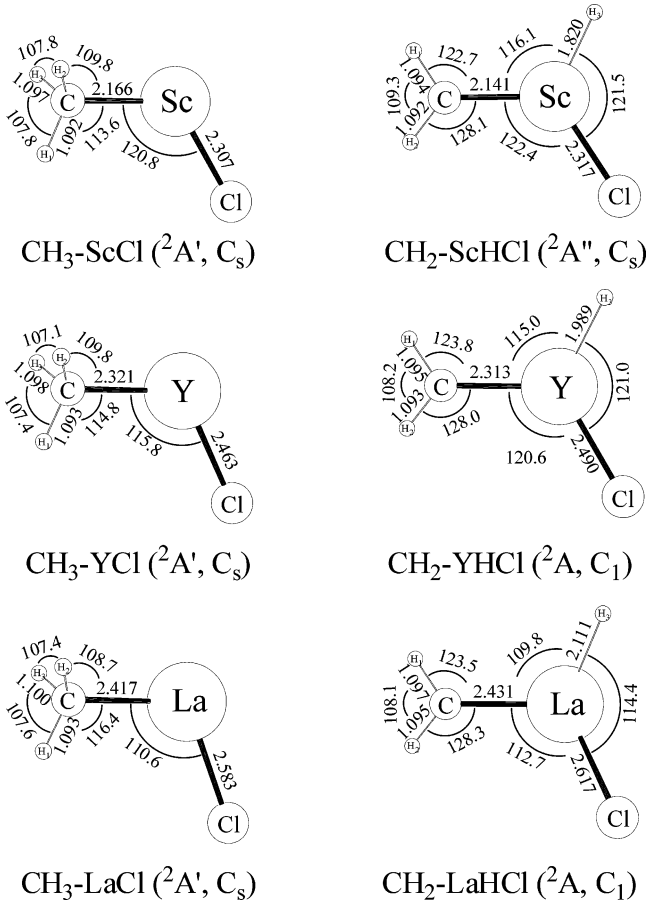

Figure 11. Optimized molecular structures of the insertion and methylidene complexes of group 3 metals with CH_3Cl calculated using B3LYP and the 6−311++G(3df,3pd) basis set. The all-electron basis is used for Sc, whereas the SDD pseudopotential and basis are used for Y and La. The bond lengths and angles are in angstroms and degrees. The electronic states and molecular symmetry are shown below the structure.

complexes. Finally, the harmonic calculated frequencies are compared for the CH_3−LaX and CH_2−LaHX products in Tables 8 and 9.

Structures. The structures of the products from reactions of group 3 metals with methyl halides investigated in this study are illustrated in Figures 10−12 and S3 (Supporting Information), and the molecular parameters are listed in Tables S3 and S4 (Supporting Information) all using the B3LYP density functional. Other levels of theory also give similar structural parameters. For comparison, the C−Sc bond length in CH_2−ScHF is 2.158 Å with BPW91, 2.181Å with MP2, and 2.163 Å with CCSD. A diagnostic in the CCSD calculation (T1, 0.014)[37] verifies that multireference character is not a problem in describing the electronic configuration. While the insertion complexes all have C_s structures, the methylidene structure varies with the metal and halogen size. The Sc and La methylidenes have planar (C_s) and C_1 structures, respectively. The Y methylidene complex has a C_1 structure with F and Cl, but a C_s structure with Br. A similar tendency is also reported in the case of group 3 metals + CH_4.[17] The La atom forms a pyramidal structure in CH_2−MHX, parallel to the case of CH_2−LaH_2, and the carbon atom builds up a plane with the two hydrogen and metal atoms.

It is interesting that the methylidene complexes show no agostic distortion, such as the group 3 metal methylidene dihydrides.[17] Agostic distortion is common in the structure of alkylidene complexes of early transition metals[38] and even more obvious in the structures of the small methylidene complexes of group 4−6 metals.[15] More recent theoretical study by von Frantzius et al. also reproduced the agostic structure of Ti methylidene hydride fluoride.[39] The absence of agostic distortion in the group 3 methylidenes demonstrates the importance of the number of valence electrons, which affects the electron density in the carbon−metal bond and limits it to a single bond with no agostic interaction.

Figures 10−12 also show that the C−M bond lengths of the methylidene complexes are comparable to those of the insertion complexes, indicating that the methylidene C−M bonds are basically single bonds. Similar results are also observed from the insertion and methylidene hydride complexes from reactions of group 3 metals and methane. In group 4−6 metal systems, the C−M bond length of the high oxidation state complex is normally more than 0.2 Å shorter than that of the insertion complex, indicating that the carbon−metal bond is a multiple bond.

The two structural characteristics of the group 3 metal complexes, no agostic distortion and the relatively long methylidene C−M bond length, most likely share the same origin. Recent studies of small methylidene complexes from reactions of early transition metals with CH_4 and CH_3X have shown that more electron density of the methylidene C−M bond normally leads to a shorter bond and more agostic distortion.[15] The C−M bonds of the group 3 metal methylidenes are the longest among those of the early transition-metal methylidenes, and the small number of valence electrons does not allow for the formation of a multiple bond between the carbon and metal atoms.

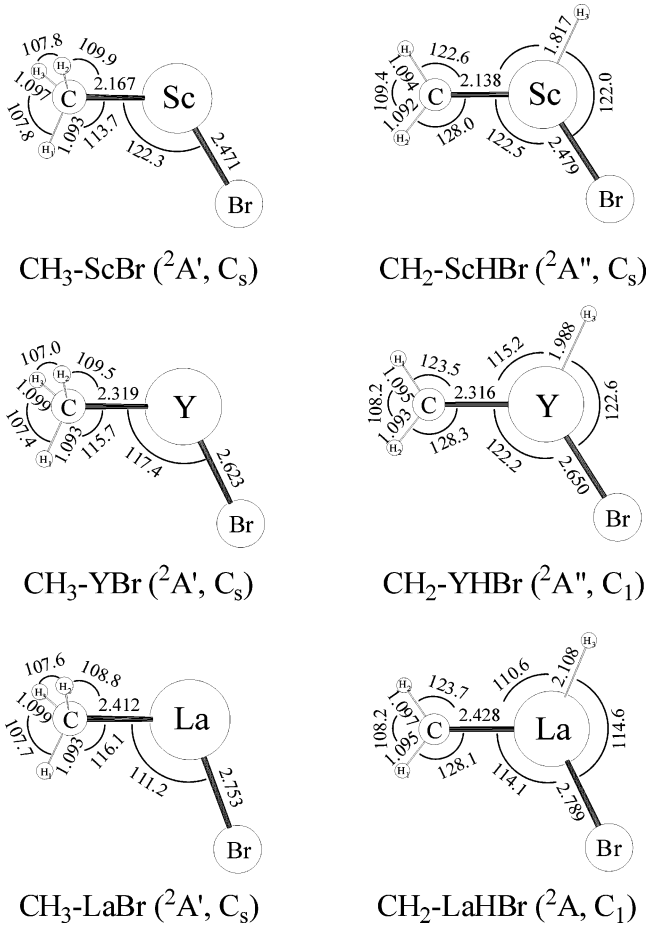

Figure 12. Optimized molecular structures of the insertion and methylidene complexes of group 3 metals with CH_3Br calculated using B3LYP and the 6−311++G(3df,3pd) basis set. The all-electron basis is used for Sc, whereas the SDD pseudopotential and basis are used for Y and La. The bond lengths and angles are in angstroms and degrees. The electronic states and molecular symmetry are shown below the structure.

The agostic interaction is currently understood as delocalization of the carbon−metal bonding electrons,[38] and therefore, the electron density in the bond is an important probe for the magnitude of the interaction. The extent of agostic distortion in small methylidene complexes varies progressively with the number of valence electrons of the metal atom and the ligand electronegativity.[9−11,15] The present results reconfirm the importance of the number of metal valence electrons on the magnitude of agostic distortion for small CH_2−MHF methylidenes. This trend is displayed in Figure 2 of our recent review article.[15]

Looking closely at the molecular structures in Figures 10−12, the C−Sc bond of the insertion complex is shorter relative to that of the methylidene complex, regardless of the halogen size. For instance, the C−M bond of CH_3−MF is 0.013, 0.002, and −0.014 Å longer in the order of Sc, Y, and La than that of CH_2−MHF. The same tendency is also observed in the Group 3 metal + CH_4 cases.[17] The CH_3−ScX complex has an unpaired electron on the Sc atom, whereas the methylidene complex contains the extra electron density mostly on the carbon atom.

The observed tendency in the relative C−M bond lengths between CH_3−MX and CH_2−MHX suggests that electron donation of the unpaired electron of the carbon atom of CH_2−MHX to the empty d-orbital of the metal atom decreases with increasing atomic weight of the metal. In the case of CH_2−MHF, the spin density of the metal atom decreases with increasing atomic mass of the metal, 0.109, 0.092, and 0.077, while that of the carbon atom increases, 0.944, 0.955, and 0.961, respectively. This arises from less effective C(2p)−M(nd) overlap with increasing metal size. Notice also that spin densities on the hydrogen atoms bonded to carbon are slightly negative due to spin polarization from the carbon π radical and the spin densities of the metal hydride and halide substituents are very, very small (Table S4, Supporting Information). Finally, there is a general decrease in C−M bond length with increasing halogen substituent size for the group 3 metals and early transition metals as well.[15]

Conclusions

Reactions of laser-ablated group 3 metal atoms with methyl halides (X = F, Cl, and Br) were carried out and the matrix infrared spectra studied. Three sets of product absorptions marked **i**, **m**, and **h** are observed and grouped on the basis of the behaviors upon photolysis and annealing. Visible and UV photolysis normally favor the **i** and **m** absorptions, respectively, while detail variations depend on the metal and halogen. In several systems the **i** and **m** absorptions are photoreversible. The **h** absorptions increase substantially at high concentration but only slightly on photolysis and annealing. The **i**, **m**, and **h** absorptions are attributed to the insertion (CH_3−MH), methylidene dihydride (CH_2−MH_2), and higher-order (CH_3MX_2) products. The yield of the higher-order complex decreases with the atomic weight of the metal.

The C−M bond length of CH_2−MHX is comparable to that of CH_3−MH, indicative of essentially a single bond, in contrast to those of the methylidene complexes formed from group 4−6 metals.[9−15] There is evidence for weak C(2p)−Sc(3d) π bonding in the CH_2−ScHX complexes. It is interesting that the group 3 metal methylidene complexes are not agostically distorted, consistent with the group 3 metal methylidene dihydrides,[17] but clearly different from the methylidene complexes of group 4−6 metals.[15] The relatively long C−M bond and no agostic distortion of the methylidene complexes are traced to the small number of valence electrons in the group 3 metal, resulting in a low electron density in the essentially single C−M bond. The present results reconfirm the trend that more electron density in the carbon−metal bond of the small methylidene complex normally leads to more distortion around the bond due to stronger agostic interaction.[15]

Acknowledgment. We gratefully acknowledge financial support from NSF Grant CHE 03-52487 to L.A. and valuable encouragement from Marjorie Hare Andrews.

Supporting Information Available: Figures S1−S3, showing IR spectra and optimized molecular structures, and Tables S1−S4, listing harmonic frequencies and geometrical parameters. This material is available free of charge via the Internet at http://pubs.acs.org.

References and Notes

(1) (a) Haiduc, I.; Zuckerman, J. J. *Basic Organometallic Chemistry*; Walter de Gruyter: New York, NY, 1985. (b) Crabtree, R. H. *The Organometallic Chemistry of the Transition Metals*; John Wiley & Sons: Hoboken, NJ, 2005.

(2) (a) Hayes, P. G.; Piers, W. E.; McDonald, R. *J. Am. Chem. Soc.* **2002**, *124*, 2132. (b) Hayes, P. G.; Piers, W. E.; Lee, L. W. M.; Knight, L. K.; Parvez, M.; Elsegood, M. R. J.; Clegg, W. *Organometallics* **2001**, *20*, 2533. (c) Bulls, A. R.; Bercaw, J. E.; Manriquez, J. M.; Thompson, M. E. *Polyhedron* **1988**, *7*, 1409. (d) Perry, J. K.; Goddard, W. A., III. *J. Am. Chem. Soc.* **1994**, *116*, 5013.

(3) (a) Sunerlin, L. S.; Armentrout, P. B. *J. Am. Chem. Soc.* **1989**, *111*, 3845. (b) Huang, Y.; Wise, M. B.; Jacobson, D. B.; Freiser, B. S. *Organometallics*, **1987**, *6*, 346.

(4) (a) Siegbahn, P. E. M.; Svensson, M. *Chem. Phys. Lett.* **1993**, *216*, 147. (b) Siegbahn, P. E. M.; Blomberg, M. R. A.; Svensson, M. *J. Am. Chem. Soc*. **1993**, *115*, 4191. (c) Blomberg, M. R. A.; Siegbahn, P. E. M.; Svensson, M. *J. Am. Chem. Soc.* **1992**, *114*, 6095.

(5) Siegbahn, P. E. M.; Blomberg, M. R. A. *Organometallics* **1994**, *13*, 354. (MX + CH_4).

(6) Vidal, I.; Melchor, S.; Dobado, J. A. *J. Phys. Chem. A* **2005**, *109*, 7500.

(7) Dalmázio, I.; Duarte, H. A. *J. Chem. Phys.* **2001**, *115*, 1747.

(8) Bauschlicher, C. W., Jr.; Partridge, H.; Sheehy, J. A.; Langhoff, S. R.; Rosi, M. *J. Am. Chem. Soc.* **1992**, *96*, 6969.

(9) (a) Cho, H.-G.; Andrews, L. *J. Phys. Chem. A* **2004**, 108, 6294. (Ti + CH_3F). (b) Cho, H.-G.; Andrews, L. *Inorg. Chem*. **2005**, *44*, 979 (Ti + CH_3X). (c) Cho, H.-G.; Andrews, L. *J. Am. Chem. Soc*. **2004**, *126*, 10485. (Zr + CH_3F). (d) Cho, H.-G.; Andrews, L. *Organometallics* **2004**, *23*, 4357. (Hf + CH_3F). (e) Cho, H.-G.; Andrews, L. *Chem. Asian J*. **2006**, *1*, 404 (Zr and Hf + CH_3X).

(10) (a) Cho, H. G.; Andrews, L. *Organometallics* **2005**, *24*, 477. (Nb + CH_3F). (b) Cho, H.-G.; Andrews, L. *J. Phys. Chem. A* **2006**, *110*, 10063. (V, Nb, and Ta + CH_3X).

(11) (a) Cho, H.-G.; Andrews, L. *Chem. Eur. J* **2005**, *11*, 5017. (Mo + CH_3F). (b) Cho, H.-G.; Andrews, L. *Organometallics* **2005**, *24*, 5678. (Cr and W + CH_3F).

(12) (a) Andrews, L.; Cho, H.-G.; Wang, X. *Inorg. Chem*. **2005**, *44*, 4834. (Ti + CH_4). (b) Cho, H.-G.; Wang, X.; Andrews, L. *Organometallics* **2005**, *24*, 2854. (Hf + CH_4). (c) Andrews, L.; Cho, H.-G.; Wang, X. *Angew. Chem., Int. Ed*. **2005**, *44*, 113. (Zr + CH_4). (d) Cho, H.-G.; Wang, X.; Andrews, L. *J. Am. Chem. Soc*. **2005**, *127*, 465. (Zr + CH_4).

(13) Cho, H. G.; Andrews, L. *J. Phys. Chem.* **2006**, *110*, 3886. (V, Nb, and Ta + CH_4).

(14) (a) Cho, H.-G.; Andrews, L. *J. Am. Chem. Soc*. **2005**, *127*, 8226. (Mo + CH_4). (b) Cho, H.-G.; Andrews, L.; Marsden, C. *Inorg. Chem.* **2005**, *44*, 7634. (Cr and W + CH_4).

(15) Andrews, L.; Cho, H.-G. *Organometallics* **2006**, *25*, 4040. (Review article).

(16) (a) Schrock, R. R. *Chem. Rev.* **2002**, *102*, 145. (b) Buchmeiser, M. R. *Chem. Rev.* **2000**, *100*, 1565.

(17) Cho, H. G.; Andrews, L. *Organometallics* **2007**, *26*, 633.

(18) (a) Zhou, M. F.; Andrews, L. *J. Phys. Chem. A* **1998**, *102*, 8251. (b) Wang, X.; Andrews, L. *J. Phys. Chem. A* **2003**, *107*, 570.

(19) Andrews, L.; Citra, A. *Chem. Rev*. **2002**, *102*, 885, and references cited therein.

(20) Kudin, K. N.; Burant, J. C.; Millam, J. M.; Iyengar, S. S.; Tomasi, J.; Barone, V.; Mennucci, B.; Cossi, M.; Scalmani, G.; Rega, N.; Petersson, G. A.; Nakatsuji, H.; Hada, M.; Ehara, M.; Toyota, K.; Fukuda, R.; Hasegawa, J.; Ishida, M.; Nakajima, T.; Honda, Y.; Kitao, O.; Nakai, H.; Klene, M.; Li, X.; Knox, J. E.; Hratchian, H. P.; Cross, J. B.; Adamo, C.; Jaramillo, J.; Gomperts, R.; Stratmann, R. E.; Yazyev, O.; Austin, A. J.; Cammi, R.; Pomelli, C.; Ochterski, J. W.; Ayala, P. Y.; Morokuma, K.; Voth, G. A.; Salvador, P.; Dannenberg, J. J.; Zakrzewski, V. G.; Dapprich, S.; Daniels, A. D.; Strain, M. C.; Farkas, O.; Malick, D. K.; Rabuck, A. D.; Raghavachari, K.; Foresman, J. B.; Ortiz, J. V.; Cui, Q.; Baboul, A. G.; Clifford, S.; Cioslowski, J.; Stefanov, B. B.; Liu, G.; Liashenko, A.; Piskorz, P.; Komaromi, I.; Martin, R. L.; Fox, D. J.; Keith, T.; Al-Laham, M. A.; Peng, C. Y.; Nanayakkara, A.; Challacombe, M.; Gill, P. M. W.; Johnson, B.; Chen, W.; Wong, M. W.; Gonzalez, C.; Pople, J. A. *Gaussian 03*, Revision B.04; Gaussian: Pittsburgh, PA, 2003.

(21) (a) Becke, A. D. *J. Chem. Phys.* **1993**, *98*, 5648. (b) Lee, C.; Yang, Y.; Parr, R. G. *Phys. Rev. B* **1988**, *37*, 785.

(22) Raghavachari, K.; Trucks, G. W. *J. Chem. Phys*. **1989**, *91*, 1062.

(23) Andrae, D.; Haeussermann, U.; Dolg, M.; Stoll, H.; Preuss, H. *Theor. Chim. Acta* **1990**, *77*, 123.

(24) Page, M.; Doubleday, C.; McIver, J. W., Jr. *J. Chem. Phys*. **1990**, *93*, 5634.

(25) Burke, K.; Perdew, J. P.; Wang, Y. In *Electronic Density Functional Theory: Recent Progress and New Directions*; Dobson, J. F., Vignale, G., Das, M. P., Eds.; Plenum: London, 1998.

(26) Frisch, M. J.; Head-Gordon, M.; Pople, J. A. *Chem. Phys. Lett.* **1990**, *166*, 281.

(27) Pople, J. A.; Krishnan, R.; Schlegel, H. B.; Binkley, J. S. *Int. J. Quantum Chem.* **1978**, *14*, 545.

(28) (a) Wang, X.; Chertihin, G. V.; Andrews, L. *J. Phys. Chem. A* **2002**, *106*, 9213. (b) Wang, X.; Andrews, L. *J. Am. Chem. Soc.* **2002**, *124*, 7610.

(29) (a) Huber, K. P.; Herzberg, G. *Molecular Spectra and Molecular Structure*; Van Nostrand Reinhold: New York, 1979. (b) Langhoff, S. R.; Bauschicher, C. W., Jr.; Partridge, H. *J. Chem. Phys.* **1988**, *89*, 369.

(30) Shenyavskaya, E. A.; Ross, A. J.; Topouzkhanian, A.; Wannous, G. *J. Mol. Spectrosc*. **1993**, *162*, 327. (ScF).

(31) McLeod, D., Jr.; Weltner, W., Jr. *J. Chem. Phys.* **1966**, *70*, 3293.

(32) (a) Hastie, J. W.; Hauge, R. H.; Margrave, J. L. *J. Less-Common Met*. **1975**, *39*, 309. (MF_3). (b) Wesley, R. D.; DeKock, C. W. *J. Chem. Phys.* **1973**, *77*, 466. (LaF_3).

(33) (a) McGrady, G. S.; Downs, A. J.; Bednall, N. C.; McKean, D. C.; Thiel, W.; Jonas, V.; Frenking, G.; Scherer, W. *J. Phys. Chem. A* **1997**, *101*, 1951. (b) McGrady, G. S.; Down, A. J.; McKean, D. C.; Haaland, A.; Scherer, W.; Verne, H.-P.; Volden, H. V. *Inorg. Chem*. **1996**, *35*, 4713. (c) Kaupp, M. *Chem. Eur. J.* **1999**, *5*, 3631.

(34) Andrews, L.; Zhou, M. F.; Chertihin, G. V.; Bauschlicher, C. W., Jr. *J. Phys. Chem. A* **1999**, *103*, 6525.

(35) (a) Wesley, R. D.; DeKock, C. W. *J. Phys. Chem*. **1973**, *77*, 466. (YF_2 and YF_3).

(36) (a) Hildenbrand, D. L.; Lau, K. H. *J. Chem. Phys.* **1995**, *102*, 3769. (b) Solomonic, V. G.; Stanton, J. F.; Boggs, J. F. *J. Chem. Phys.* **2005**, *122*, 94322.

(37) Lee, T. J.; Taylor, P. R. *Int. J. Quantum Chem. Symp.* **1989**, *23*, 199.

(38) (a) Scherer, W.; McGrady, G. S. *Angew. Chem., Int. Ed.* **2004**, *43*, 1782. (b) Clot, E.; Eisenstein, O. Agostic Interactions from a Computational Perspective. In *Structure and Bonding, Computational Inorganic Chemistry*; Kaltzoyannis, N., McGrady, E., Eds.; Springer-Verlag: Heidelberg, Germany, 2004; pp 1−36.

(39) von Frantzius, G.; Streubel, R.; Brandhorst, K.; Grunenberg, J. *Organometallics* **2006**, *25*, 118.